JOURNAL OF SYNCHROTRON RADIATION

ISSN 1600-5775

Received 23 January 2018
Accepted 6 June 2018

Edited by I. Schlichting, Max Planck Institute for Medical Research, Germany

Keywords: photo-electron spectroscopy; HAXPES; beamline; Indus-2; bending magnet.

HAXPES beamline PES-BL14 at the Indus-2 synchrotron radiation source

Jagannath, U. K. Goutam,* R. K. Sharma, J. Singh, K. Dutta, U. S. Sule, R. Pradeep and S. C. Gadkari

Technical Physics Division, Bhabha Atomic Research Centre, Trombay, Mumbai, India.
*Correspondence e-mail: ukgoutam@rrcat.gov.in

The Hard X-ray Photo-Electron Spectroscopy (HAXPES) beamline (PES-BL14), installed at the 1.5 T bending-magnet port at the Indian synchrotron (Indus-2), is now available to users. The beamline can be used for X-ray photoemission electron spectroscopy measurements on solid samples. The PES beamline has an excitation energy range from 3 keV to 15 keV for increased bulk sensitivity. An in-house-developed double-crystal monochromator [Si (111)] and a platinum-coated X-ray mirror are used for the beam monochromatization and manipulation, respectively. This beamline is equipped with a high-energy (up to 15 keV) high-resolution (meV) hemispherical analyzer with a microchannel plate and CCD detector system with *SpecsLab Prodigy* and *CasaXPS* software. Additional user facilities include a thin-film laboratory for sample preparation and a workstation for on-site data processing. In this article, the design details of the beamline, other facilities and some recent scientific results are described.

1. Introduction

Ever since the realization of the analytical potential of X-ray photoelectron spectroscopy (XPS) as a technique by Siegbahn's group, this powerful, non-destructive analytical tool has made significant contributions to the basic understanding of the surface electronic and band structures of atoms and molecules in solids (Siegbahn *et al.*, 1967). In particular, XPS has been effectively utilized in the characterisation of material surfaces and in specific areas of materials science such as adhesion, polymer chemistry, corrosion and composite materials, and has also been widely used to investigate structure and composition, reaction mechanisms, poisoning and reactivation *etc*. on the surfaces of catalysts as well as gas sensor materials (Briggs, 1977; Watts, 1994; Katti *et al.*, 2003). Although, the XPS technique based on conventional (laboratory) sources has proved to be one of the powerful analytical probes in surface science studies, it has posed severe problems in the investigation of the electronic and chemical states of bulk nanostructures and buried interfaces (even at depths of ~10 nm) that is useful in the advancement of many semiconductor devices (Kobayashi, 2005). On the other hand, the discovery of synchrotron radiation, and the unique properties offered by such sources that are not offered by conventional ones, such as continuity, tunability, wide photon energy range (infrared to hard X-rays), high brilliance, excellent polarization characteristics and a high degree of angular collimation (hence, resolution), has led to the construction of several dedicated synchrotron radiation facilities around the world for conducting a wide range of experiments in various scientific disciplines such as physics,

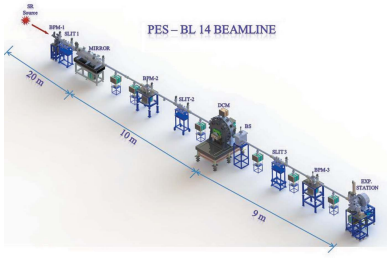

chemistry, biophysics, materials sciences, *etc.* (Margaritondo, 1988; Mills, 2002). The high-energy source in XPS, for instance, increases the kinetic energy of emitted photoelectrons; thus, the inelastic mean free-path (IMFP) of electrons is known to exceed 10 nm for several materials (Takata *et al.*, 2005). Hence, an intrinsic bulk-sensitive XPS probe can be realized by increasing the kinetic energy of photoelectrons by the use of hard X-rays that are readily available at synchrotron radiation facilities. The first feasibility test of the XPS technique using a synchrotron radiation source was carried out by Lindau and co-workers (Lindau *et al.*, 1974). Using a bending magnet (BM) based on a first-generation synchrotron radiation source, they demonstrated the possibility of detecting photoelectrons with up to 8 keV of kinetic energy, and showed that high-resolution XPS could be profitably carried out in the hard X-ray energy range of 5–15 keV with synchrotron radiation. However, the full-scale experimental utilization of the high energy resolution and high-throughput XPS technique using hard synchrotron radiation X-rays was realized only with the availability of extremely high brilliance third-generation synchrotron radiation sources and high-performance electron energy analyzers (Braicovich *et al.*, 1997; Fèvre *et al.*, 1998).

In recent years, the hard X-ray photo-electron spectroscopy technique (HXPES) has been effectively utilized to differentiate between the electronic structures of the bulk and the surface of a material as well as to chemically characterize buried layers (or other deep-lying structures) that are of interest for certain device applications (Horiba *et al.*, 2004; Sato *et al.*, 2004; Chainani *et al.*, 2004; Takata *et al.*, 2004). Furthermore, the availability of high-brilliance synchrotron radiation sources coupled with a resolution of less than 0.1 eV obtained even for hard X-rays with energies >5 keV has extended the capability of the XPS technique not just to probe the bulk electronic structures of core levels but also to record the corresponding high-resolution valence band spectra of solids (Kobayashi *et al.*, 2003; Sekiyama *et al.*, 2000; Fadley, 2005). A few research groups have recently exploited these features by applying HXPES to many interesting materials from the point of view of both basic and applied research (Dallera *et al.*, 2004; Torelli *et al.*, 2005). Their work clearly indicates a wide range of applications for the XPS technique using synchrotron radiation, and these include depth-resolved electronic structure, buried layers, interfaces, ultrashallow junctions and the bulk electronic structure of strongly correlated electron systems (Kobayashi, 2005).

The Indus-2 synchrotron is an electron storage ring (Ghodke *et al.*, 2006) designed for 2.5 GeV beam energy and stores current up to 200 mA (Ghodke & Hannurkar, 2014) at Raja Ramanna Center for Advanced Technology (RRCAT), Indore, India. It is operated in decay mode with a typical lifetime of ∼22 h at 100 mA of stored beam current (Kumar *et al.*, 2013). The storage ring operates with horizontal and vertical beam emittance of 58 nm rad and 0.58 nm rad, respectively. Recently, Indus-2 has been upgraded to a third-generation source with the commissioning of two undulators (Hannurkar, 2015). HXPES beamlines devoted to high-resolution studies have been set up at most synchrotron sources in recent years because of their unique characteristics such as enabling the user to extract almost complete information about the elemental as well as chemical states of materials *etc.*, with increased bulk sensitivity. In view of this, we have also developed an HXPES beamline utilizing a large energy range (3–15 keV) of synchrotron radiation from the bending magnet of a third-generation synchrotron source at Indus-2 at RRCAT, Indore, India. This beamline is a national facility and the Department of Atomic Energy (DAE), Government of India, has funded its construction and operation. The PES-BL14 beamline is primarily aimed to cater to the needs of research groups in India working in the area of solid-state basic and applied research. The beamline is designed to provide hard X-rays for high-resolution studies of atomic and electronic structures of surfaces and interfaces with increased bulk sensitivity. The first high-resolution XPS data of a gold sample were recorded during November 2017 and since then the beamline has been used by several researchers.

2. Beamline overview

2.1. Photon source and the front-end

The photon source for this beamline is a 1.5 T bending magnet located at port No. 14 (10° port) of the Indus-2 synchrotron radiation source. The beamline front-end (FE) (Raghuvanshi *et al.*, 2007), which finishes at 16 m from the source, has most of its components inside the thick concrete wall of the Indus-2 ring. The FE consists of a fixed-exit copper mask that provides a 3 mrad horizontal aperture and allows full vertical size for the white beam. The FE also contains various pneumatic gate valves and water-cooled shutters including the safety shutter and the fast-closing shutter. The FE makes use of the fast-closing shutter and a delay line for ultrahigh-vacuum (UHV) protection of the storage ring. The 200 µm-thick beryllium window at the end of the FE separates the storage ring vacuum from that of the beamline. It also acts as a high-pass filter, removing photons with energies less than 3 keV, thus reducing the heat load on the downstream optical components.

2.2. Beamline optics

The beamline is 39 m long starting from the bending-magnet source to the sample position and is operated under UHV (10^{-9} mbar) conditions. It comprises several components, namely slits (three sets), a toroidal mirror (TM), three beam-position monitors (BPMs), a double-crystal monochromator (DCM), a beam shutter (BS) and an experimental station as depicted schematically in Fig. 1. All these components are water-cooled (297 ± 0.5 K), except the experimental station. Lead-shielded hutches and interlocked doors are provided to protect users from ionizing radiation. The primary slit is placed just after the FE to select the central cone of the X-ray beam for the TM with optimal dimensions (the angular beam size was taken to be 3 mrad × 0.4 mrad, so at 20 m from the source the slit width was fixed at 60 mm × 8 mm). The

profile and the position of the X-ray beam after the primary slit are measured by BPM-1. All BPMs are equipped with a phosphor-coated water-cooled copper block with an electrically isolated tungsten wire attached at the bottom. The vertical beam profile, measured from the photocurrent, is generated by scanning the tungsten wire through the X-ray beam. The white X-ray beam shines at an incident angle of 9 mrad on the surface of the TM reflecting it upwards. The TM is a platinum-coated 1.1 m-long single piece of silicon crystal, which ensures a flat reflectivity response for the X-rays in the working energy range of the beamline. The TM improves the energy resolution by collimating the X-ray beam in the vertical plane and focusing it in the horizontal plane. BPM-2, installed immediately after the TM, is used for the alignment of the beam in the beamline.

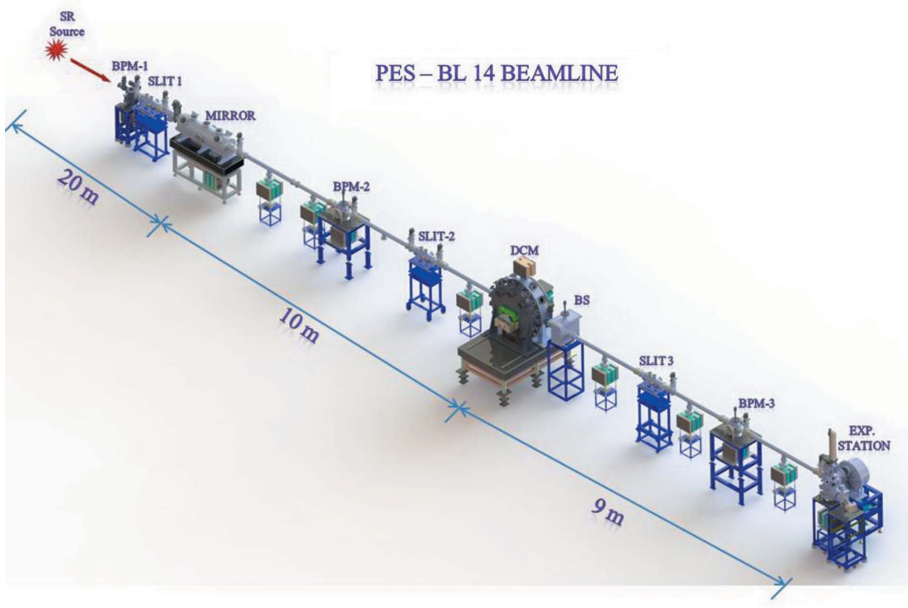

Figure 1
Schematic layout of the PES-BL14 beamline showing different optical and diagnostic components such as slits, the toroidal mirror chamber, the double-crystal monochromator, beam position monitors *etc.*

An in-house-developed DCM (Jagannath *et al.*, 2007) is installed at 20 m from the source and provides a tunable monochromatic X-ray beam with energy ranging from 3 keV to 15 keV. The DCM uses a pair of flat Si crystals in (+, −) configuration, which ensures constant exit beam height and angle. The DCM consists of a pair of crystals, Si(111), and has the provision to accommodate another pair for future upgrade. These pairs can be exchanged in-vacuum as per the user requirement for resolution. In a vacuum chamber the crystals are mounted on motorized X–Y–Z stages which are on the goniometer (Huber make) for angular rotation and hence energy selection. The necessary angular tilts of the second crystal that are needed to suppress higher harmonics have been evaluated and incorporated through a tilting assembly mounted on X–Y stages. The complete DCM software, including the motorized movements of the X–Y–Z with encoder, rotation with the goniometer, tilting with linear variable differential transformer (LVDT) feedback, has been developed in Microsoft Visual Basic programming language. The ultimate energy resolution of the beamline is governed by Si(111) crystals and is $\sim 1.5 \times 10^{-4}$ ($\Delta E/E$). A beam shutter (photon shutter) is placed downstream from the DCM in the optics hutch which allows the experimental hutch to be entered for changing samples or carrying out alignment, opening the experimental hutch without closing the main safety shutter in the FE so that the beam remains available in the optics hutch, thus keeping the optical components under steady heat load (Rosenbaum *et al.*, 2006). Finally, the monochromatic beam is focused at the sample in the experimental station placed at 39 m from the source. The toroidal mirror movement is controlled by three motorized actuators, which are controlled through a computer. The beamline components, such as the slits, mirror chambers along with actuators, beam pipes, support tables and BPMs, were designed and developed locally. The TM and the cooling systems were built by SESO, France. The beamline parameters are summarized in Table 1.

Table 1
Beamline details.

Beamline name	PES-BL14
Source type	1.5 T bending magnet
Mirror	TM: 1.1 m long, single-crystal Si with Pt coating
Monochromator	Water-cooled DCM with a pair of Si(111) crystals
Energy range (keV)	3–15
Beam size (mm) (FWHM)	4 × 1 (H × V)
Flux (photons s^{-1})†	9.16×10^9
Resolution ($\Delta E/E$)	1.5×10^{-4}
Analyzer	Phoibos 225 (0–15 keV) (mean radius 225 mm)
Detector	MCP (40 mm), CCD (Peltier-cooled)

† Measured using a calibrated AXUV 100 photodiode placed close to the sample position. The slit opening was 1 mm × 1 mm and the X-ray energy was 7 keV, while the storage ring parameters were 2.5 GeV and 100 mA.

2.3. Experimental station

The experimental station mainly consists of a vacuum chamber, sample manipulator, a hemispherical analyzer and detector system with high-voltage power supplies (Phoibos 225, Specs, Germany). The typical pressure in the experimental station is 5×10^{-9} mbar. The sample manipulator has five axes (VG Scienta) with rotations about the z- and tilt axes. The temperature range of the sample manipulator, in heating, is 1000°C, and in cooling can go down to liquid-nitrogen temperature (77 K). A photograph of the experimental station is shown in Fig. 2. The Specs Phoibos 225 hemispherical electrostatic energy analyzer allows recording of energy

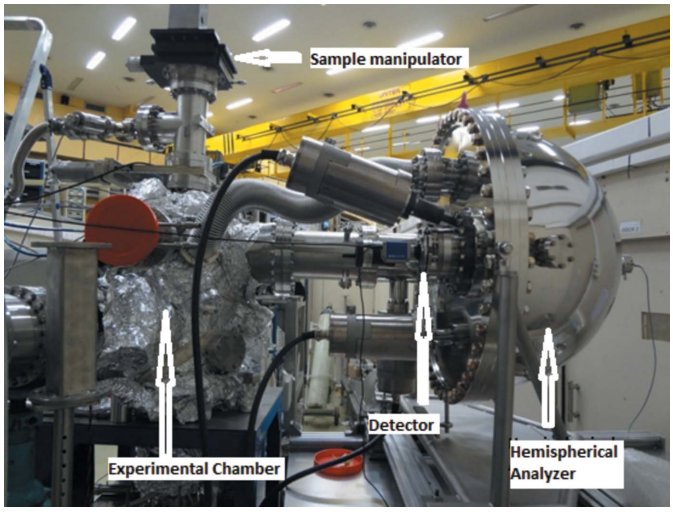

Figure 2
Experimental station of the PES beamline, depicting the experimental chamber, hemispherical analyzer (Phoibos 225) and detector, *etc*.

spectra for negative particles (electrons) and positive particles (ions) in the kinetic energy range from 0 eV to 15 keV. The Phoibos 225 has a mean radius of 225 mm. The input lens is designed to accommodate a wide range of applications. The energy resolution of the analyser is 60 meV at 15 keV. The 2D-CCD detector features a 12 bit digital Peltier-cooled camera with a dynamic range of 1000. The Peltier-cooled camera shows a significantly lower thermal noise compared with a standard CCD camera. This makes this detector most suitable for low-count-rate applications with long exposure times. A multi-element two-stage transfer lens can be operated in several different modes for angular and spatially resolved studies. All lens modes can be set electronically. A slit-orbit mechanism and a multi-mode lens make the sampling area of the analyzer and the acceptance angle area of the lens selectable. Thus, the analyzer allows spatially resolved measurements down to a diameter of 100 µm as well as large-area investigations associated with different lens acceptance angles.

The sample holder is a VG Scienta (Part No. ZSH2E50) dual-axis sample holder with sample offset capability. The samples that can be studied are solids normally in pellet form or thin films on a substrate. The sample cleaving facility is presently not available.

2.4. Experiment control and data analysis

The beamline components are remotely controlled through their respective controllers and software. Microsoft Visual Basic has been used as the primary programming language for all of the optical components of the beamline including DCM, mirror and BPMs. The software for operating the DCM and the slits was developed in-house whereas that for operating the BPMs was supplied by Excel Instruments Ltd (India). Data acquisition through a hemispherical analyzer is performed using *SpecsLab Prodigy* software. *SpecsLab2* is the main data acquisition program that can be used to operate the two-dimensional detector in the spectroscopic mode. The *HSA3500 Juggler* program controls the analyzer/power supply, and *CCDAcquire* controls the detector. *CasaXPS* is used for data analysis. Support related to the data acquisition and data processing is provided to the users whenever required.

3. Ancillary facilities

An auxiliary thin-film laboratory, adjacent to the beamline, has been set up for the PES-BL14 users for thin-film deposition. The laboratory is equipped with all the necessary instrumentation, which includes two thermal evaporation deposition systems, pellet preparation set-up, an ultrasonic cleaning facility, *etc*. There is also an I–V measurement setup for thin-film samples for current–voltage measurements. There is also a substrate-cleaning facility for *in situ* cleaning of the thin-film samples, and an ion etching gun is coupled with an experimental chamber for depth profiling, and an electron-flood source for charge neutralization.

4. Facility access

Facility access is available through joint collaboration with the beamline scientists or by direct submission of experimental proposals *via* the online portal (https://www.info-rrcat.ernet.in/beamline/). Beam time is allocated after review of the proposal by a scrutiny committee at RRCAT.

5. Highlights

Since commissioning, the PES-BL14 beamline is in regular operation and several research groups have collected data using this beamline. Thus far, more than 100 datasets have been collected. The first gold survey and high-resolution gold 4*f* spectra recorded at the PES-BL14 beamline are shown in Fig. 3.

Our in-house research group has used the beamline and its ancillary facilities for growth and characterization of organic thin films; some of these results are highlighted below.

5.1. Study of MgPc thin films

Magnesium phthalocyanine (MgPc), due to its low cost, mechanical flexibility and ability to form crystalline thin films at higher substrate temperatures without thermal dissociation, has played an important role in the field of organic electronics (Singh *et al.*, 2017). The performance of such thin-film devices depends particularly upon the electrical conductivity of the charge transport carriers, which are affected by the order of crystallinity, contamination and impurity concentration (Singh *et al.*, 2017). For this purpose, 20 nm thin films of MgPc were thermally evaporated on silicon substrates at room temperature and a pressure of 2.7×10^{-6} mbar. These thin films were annealed in air at 300°C and 350°C for 1 h. The high-resolution HAXPES spectra of the annealed and room-temperature (27°C) films were recorded at a pass energy of 20 eV with a step size of 0.05 eV. The aim of the present work was to

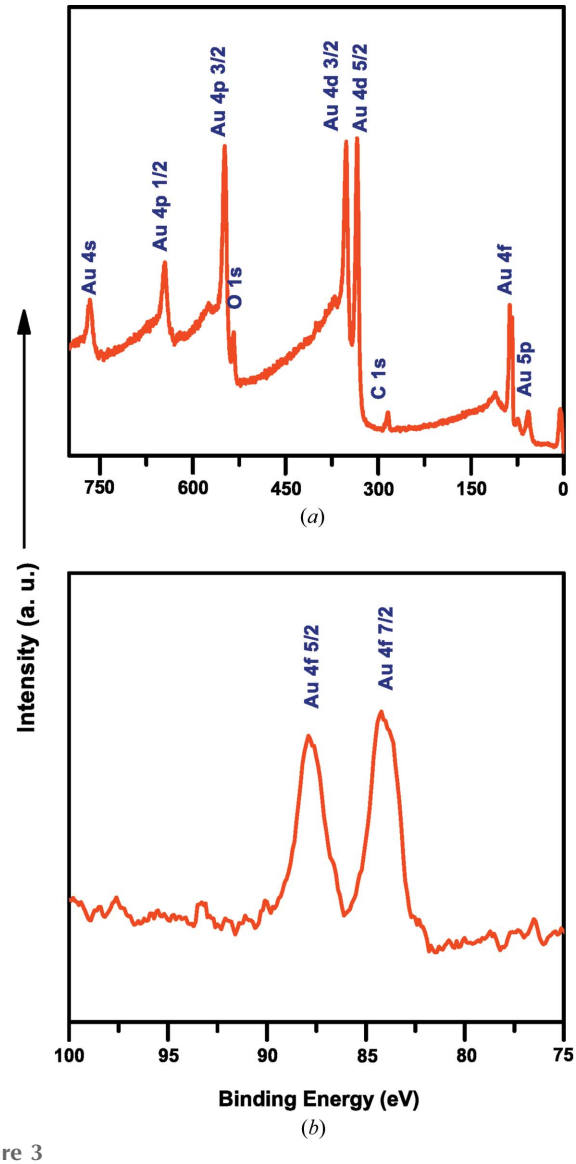

Figure 3
(*a*) A first gold survey at a step size of 0.5 eV and (*b*) gold 4*f* at a step size of 0.1 eV. Spectra was recorded at the beamline.

resolve the different types of C atoms present in the MgPc molecule in different bonding environments (Fig. 4) using high-resolution XPS measurements.

Figs. 5 and 6 show the room-temperature survey spectra and high-resolution C1*s* spectra of MgPc thin films annealed at different temperatures. All the spectra have been analyzed by means of a non-linear least-squares fit procedure using the *CasaXPS* software package. The peaks were fitted with a linear combination of Gaussian and Lorentzian functions after the subtraction of a Shirley-type background.

The low-resolution (step size of 0.2 eV at a pass energy of 100 eV) survey spectra did not resolve the different C1*s* components; however, high-resolution (step size of 0.05 eV at a pass energy of 20 eV) spectra of C1*s* clearly resolved the different components. The best fitting parameters of C1*s* spectra have been summarized in Table 2. The C1 component is the result of adventitious carbon contamination. In an MgPc

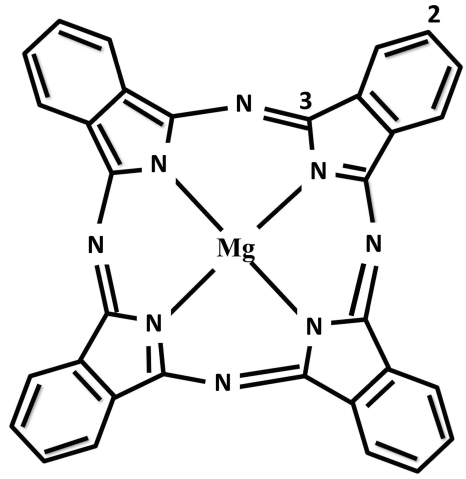

Figure 4
A magnesium phthalocyanine (MgPc) molecule. Numbers 2 and 3 denote the C atoms of the molecule with different chemical environments.

molecule, there are 32 C atoms belonging to two different chemical environments (Fig. 4). The most intense peak (C2) originates from the 24 peripheral aromatic C atoms of the benzene rings (C atoms bonded only to other C atoms). The peak (C3) on the high binding energy side comes from the eight equivalent pyrrole C atoms bridging to N atoms. The small structure (SC3) on the high binding energy side corresponds to the shakeup satellite of the C3 peak, which arises when the photoionization of the C1*s* electrons is accompanied by the simultaneous excitation of the valence electrons to an upper vacant energy level (Ouedraogo *et al.*, 1980). The positions of the C2, C3 and SC3 peaks agree with the literature

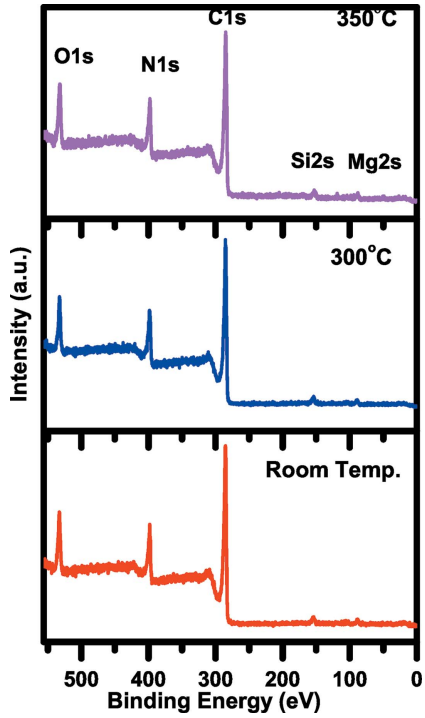

Figure 5
Survey spectra of room-temperature and annealed MgPc thin films taken at a step size of 0.2 eV at a pass energy of 100 eV.

values (Ewen *et al.*, 1991). Finally, peaks C4 and C5 are attributed to the C—OH and COOH groups of the adventitious carbon contamination.

The sum of the area ratios of the contamination peaks at 27°C, 300°C and 350°C are 0.33, 0.30 and 0.25, respectively. This decrease could be the result of an increase in the crystallinity of the films at higher annealing temperatures, which leads to more ordered MgPc molecules and a decrease in the impurity contamination in the films (Singh *et al.*, 2017). The main ordering parameter of the films is the difference (Δ) between the position of the pyrrole C1*s* peak and its satellite. From Table 2, it is clear that this difference increases with annealing temperature.

The Δ values at 27°C, 300°C and 350°C are 1.7, 2.1 and 2.5 eV, respectively. Finally, as the C2 and C3 peaks originate from the 24 and 8 C atoms, respectively, the area ratio of the C3 + SC3 and C2 peaks should therefore be 0.33. In our case, the ratios at 27°C, 300°C and 350°C are 0.6, 0.55 and 0.53, respectively. High values at a lower temperatures could be the result of overlapping of the main peaks with the contamination peaks. Also, the approach of this area ratio value to 0.33 at higher annealing temperatures can be explained by the higher structure order of the films at higher annealing temperatures. The variation of fitted C1 peak position with annealing temperature is shown in the Fig. 7.

Table 2
Best-fitting parameters for the analysis of C1*s* XPS core-level spectra.

HWHM is the half width at half-maximum.

Annealing temperature	Peak	Binding energy (eV)	HWHM (eV)	Area (total peak ratio)
Room temperature	C1	284.2	1.21	0.30
	C2	285.1	1.25	0.42
	C3	286.7	1.32	0.14
	SC3	288.4	1.30	0.11
	C5	290.5	1.31	0.03
300°C	C1	284.3	0.51	0.17
	C2	285.3	0.53	0.45
	C3	286.2	0.48	0.16
	SC3	288.3	0.50	0.09
	C4	287.1	0.52	0.13
350°C	C1	284.2	0.55	0.15
	C2	285.2	0.48	0.49
	C3	286.2	0.52	0.18
	SC3	288.7	0.51	0.08
	C4	287.4	0.53	0.10

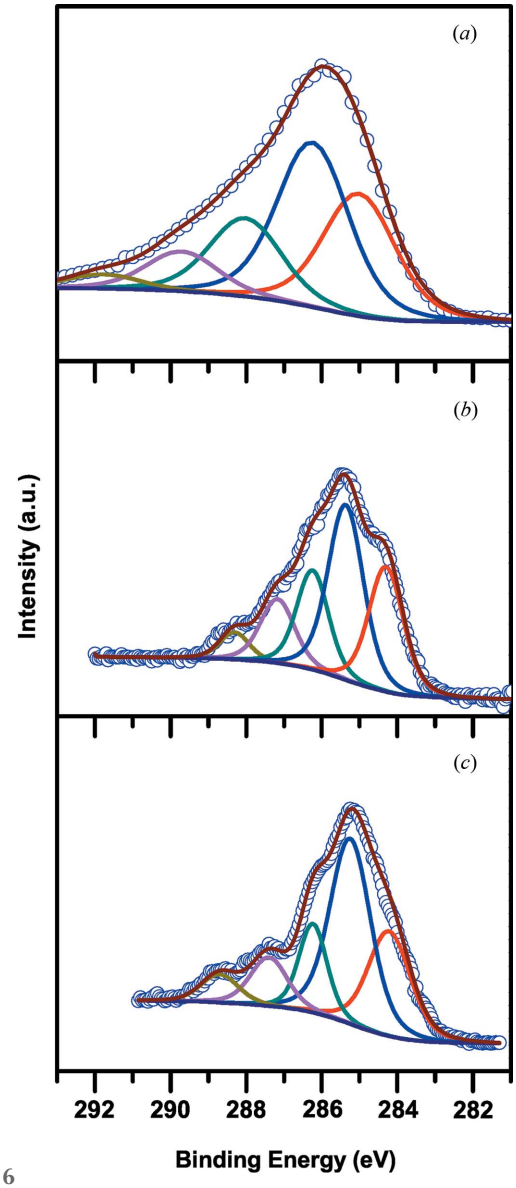

Figure 6
Fitted C1*s* room-temperature XPS spectra of MgPc thin films annealed at (*a*) room temperature, (*b*) 300°C and (*c*) 350°C.

6. Conclusions

The HAXPES beamline PES-BL14 has been installed at the bending-magnet port at the Indian synchrotron, Indus-2. The beamline can be used for hard X-ray photoemission electron spectroscopy measurements on solid samples. The PES-BL14 has a working energy range of 3–15 keV for significantly

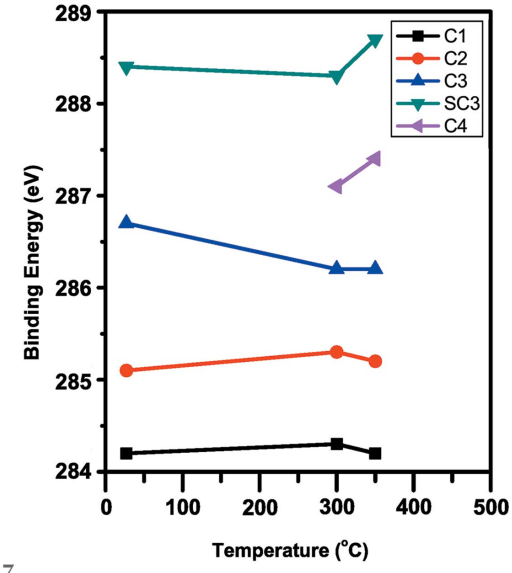

Figure 7
Variation of fitted peak position of the C1*s* XPS peak of MgPc thin films with annealing temperature.

increased sensitivity (with an information depth of more than 10 nm) which can provide information (by non-destructive means) on the bulk electronic structure or chemical composition of deeply buried interfaces. An in-house-developed DCM [Si(111)] and a platinum-coated X-ray mirror are used for beam monochromatization and manipulation, respectively. This beamline is equipped with a 15 keV high-resolution hemispherical analyzer with a microchannel plate (MCP) and CCD detector with *SpecsLab Prodigy* and *CasaXPS* software for data acquisition in different modes and processing. Additional user facilities include a thin-film laboratory for sample preparation and a workstation for on-site data processing. The PES-BL14 is capable of resolving different components of elements as demonstrated using different C1 spectra of MgPc thin films. The beamline has been commissioned recently, and since then a number of users have collected good quality datasets for different applications. In the future, we plan to incorporate another pair of crystals into the DCM to achieve better resolution for demanding applications.

Acknowledgements

The authors are thankful to the front-end and alignment team members of RRCAT for installing the front-end of PES-BL14 and helping in the alignment of some of the critical components in the beamline. Special thanks to Dr V. C. Sahni for constant encouragement and valuable discussions. We would like to acknowledge the unlimited support extended by Drs P. A. Naik, S. N. Jha, Tapas Ganguli and A. K. Sinha during installation and commissioning.

References

Braicovich, L., Brookes, N., Dallera, C., Salvietti, M. & Olcese, G. (1997). *Phys. Rev. B*, **56**, 15047–15055.

Briggs, D. (1977). Editor. *Handbook of X-ray and Ultraviolet Photoelectron Spectroscopy*. London: Heydon & Son Ltd.

Chainani, A., Yokoya, T., Takata, Y., Tamasaku, K., Taguchi, M., Shimojima, T., Kamakura, N., Horiba, K., Tsuda, S., Shin, S., Miwa, D., Nishino, Y., Ishikawa, T., Yabashi, M., Kobayashi, K., Namatame, H., Taniguchi, M., Takada, K., Sasaki, T., Sakurai, H. & Takayama-Muromachi, E. (2004). *Phys. Rev. B*, **69**, 180508.

Dallera, C., Duò, L., Braicovich, L., Panaccione, G., Paolicelli, G., Cowie, B. & Zegenhagen, J. (2004). *Appl. Phys. Lett.* **85**, 4532.

Ewen, R. J., Honeybourne, C. L. & Hill, C. A. S. (1991). *J. Phys. Condens. Matter*, **3**, S311.

Fadley, C. S. (2005). *Nucl. Instrum. Methods Phys. Res. A*, **547**, 24–41.

Ghodke, A. D. & Hannurkar, P. R. (2014). *RRCAT Newsl.* **27**, 3.

Ghodke, A. D., Husain, R., Singh, G. & Indus-2-team (2006). *Beam Dynam. Newsl.* **41**, 77–95.

Hannurkar, P. R. (2015). *RRCAT Newsl.* **28**, 3–4.

Horiba, K., Taguchi, M., Chainani, A., Takata, Y., Ikenaga, E., Miwa, D., Nishino, Y., Tamasaku, K., Awaji, M., Takeuchi, A., Yabashi, M., Namatame, H., Taniguchi, M., Kumigashira, H., Oshima, M., Lippmaa, M., Kawasaki, M., Koinuma, H., Kobayashi, K., Ishikawa, T. & Shin, S. (2004). *Phys. Rev. Lett.* **93**, 236401.

Jagannath, Sule, U. S., Pradeep, R., Sharma, R. K., Goutam, U. K., Bhandarkar, V. B., Gadkari, S. C., Yakhmi, J. V., Sahni, V. C., (2007). *Asian J. Phys.* **16** 331–338.

Katti, V. R., Debnath, A. K., Muthe, K. P., Kaur, M., Dua, A. K., Gadkari, S. C., Gupta, S. K. & Sahni, V. C. (2003). *Sens. Actuators B Chem.* **96**, 245–252.

Kobayashi, K. (2005). *Nucl. Instrum. Meth. Phys. Res. A*, **547**, 98.

Kobayashi, K., Yabashi, M., Takata, Y., Tokushima, T., Shin, S., Tamasaku, K., Miwa, D., Ishikawa, T., Nohira, H., Hattori, T., Sugita, Y., Nakatsuka, O., Sakai, A. & Zaima, S. (2003). *Appl. Phys. Lett.* **83**, 1005–1007.

Kumar, P., Ghodke, A. D. & Singh, G. (2013). *Pramana J. Phys.* **80**, 855–871.

Le Fèvre, P., Magnan, H., Chandesris, D., Vogel, J., Formoso, V. & Comin, F. (1998). *Phys. Rev. B*, **58**, 1080–1083.

Lindau, I., Pianetta, P., Doniach, S. & Spicer, W. E. (1974). *Nature (London)*, **250**, 214–215.

Margaritondo, G. (1988). *Introduction to Synchrotron Radiation*. New York: Oxford University Press.

Mills D. M. (2002). *Third-Generation Hard X-ray Synchrotron Radiation Sources: Source Properties, Optics and Experimental Techniques.* New York: John Wiley.

Ouedraogo, G. V., Benlian, D. & Porte, L. (1980). *J. Chem. Phys.* **73**, 642–647.

Raghuvanshi, V. K., Dhamgaye, V. P., Singh, A. K. & Nandedkar, R. V. (2007). *AIP Conf. Proc.* **879**, 631–634.

Rosenbaum, G., Alkire, R. W., Evans, G., Rotella, F. J., Lazarski, K., Zhang, R.-G., Ginell, S. L., Duke, N., Naday, I., Lazarz, J., Molitsky, M. J., Keefe, L., Gonczy, J., Rock, L., Sanishvili, R., Walsh, M. A., Westbrook, E. & Joachimiak, A. (2006). *J. Synchrotron Rad.* **13**, 30–45.

Sato, H., Shimada, K., Arita, M., Hiraoka, K., Kojima, K., Takeda, Y., Yoshikawa, K., Sawada, M., Nakatake, M., Namatame, H., Taniguchi, M., Takata, Y., Ikenaga, E., Shin, S., Kobayashi, K., Tamasaku, K., Nishino, Y., Miwa, D., Yabashi, M. & Ishikawa, T. (2004). *Phys. Rev. Lett.* **93**, 246404.

Sekiyama, A., Iwasaki, T., Matsuda, K., Saitoh, Y., Ônuki, Y. & Suga, S. (2000). *Nature (London)*, **403**, 396–398.

Siegbahn K., Nordling, C., Fahlman A., Nordberg R., Hamrin K., Hedman J., Johansson G., Bergmark T., Karlsson S.; Lindgren I. & Lindberg B. (1967). *ESCA: Atomic, Molecular and Solid State Structure Studied by Means of Electron Spectroscopy*. Uppasala: Almquist & Wiksells.

Singh, J., Sharma, R. K., Sule, U. S., Goutam, U. K., Gupta Jagannath & Gadkari, S. C. (2017). *Mat. Res. Express*, **4**, 076301.

Takata, Y., Tamasaku, K., Tokushima, T., Miwa, D., Shin, S., Ishikawa, T., Yabashi, M., Kobayashi, K., Kim, J. J., Yao, T., Yamamoto, T., Arita, M., Namatame, H. & Taniguchi, M. (2004). *Appl. Phys. Lett.* **84**, 4310–4312.

Takata, Y., Yabashi, M., Tamasaku, K., Nishino, Y., Miwa, D., Ishikawa, T., Ikenaga, E., Horiba, K., Shin, S., Arita, M., Shimada, K., Namatame, H., Taniguchi, M., Nohira, H., Hattori, T., Södergren, S., Wannberg, B., & Kobayashi, K. (2005). *Nucl. Instrum. Methods Phys. Res. A*, **547**, 50.

Torelli, P., Sacchi, M. & Cautero, G. (2005). *Rev. Sci. Instrum.* **76**, 023909.

Watts, J. F. (1994). *Vacuum*, **45**, 653.